Molecular Dynamics Simulations of Pentapeptides at Interfaces: Salt Bridge and Cation−π Interactions†

Marcela P. Aliste, Justin L. MacCallum, and D. Peter Tieleman*

Department of Biological Sciences, University of Calgary, 2500 University Drive NW, Calgary, Alberta, Canada T2N 1N4

Received October 14, 2002; Revised Manuscript Received May 30, 2003

ABSTRACT: Peptide−membrane interactions are important for understanding the binding, partitioning, and folding of membrane proteins; the activity of antimicrobial and fusion peptides; and a number of other processes. We describe molecular dynamics simulations (10−25 ns) of two pentapeptides Ace-WLXLL (with X = Arg or Lys side chain) (White, S. H., and Wimley, W.C. (1996) *Nat. Struct. Biol. 3*, 842−848) in water and three different membrane mimetic systems: (i) a water/cyclohexane interface, (ii) water-saturated octanol, and (iii) a solvated dioleoylphosphatidylcholine bilayer. A salt bridge is found between the protonated Arg or Lys side chains with the carboxyl terminus at the three interfaces. In water/cyclohexane, the salt bridge is most exposed to the water phase and least stable. In water/octanol and the lipid bilayer systems, the salt bridge once formed persists throughout the simulations. In the lipid bilayer, the salt bridge is more stable when the peptide penetrates deeper into the bilayer. In one of two peptides, a cation−π interaction between the Arg and the Trp side chains is stable in the lipid bilayer for about 15 ns before breaking. In all cases, the conformations of the peptides are restricted by their presence at the interface and can be assigned to a few major conformational clusters. Side chains facing the water phase are most mobile. In the lipid bilayer, the peptides remain in the interface area, where they overlap with the carbonyl area of the lipid bilayer and perturb the local density profile of the bilayer. The tryptophan side chain remains in the water−lipid interface, where it interacts with the lipid choline group and forms hydrogen bonds with the ester carbonyl of the lipid and with water in the interface.

Membrane proteins play an important role in a wide range of biological functions, including respiration, signal transduction, and molecular transport. Understanding the interactions between peptides or proteins and the membrane is fundamental to understanding membrane protein folding and the prediction of the three-dimensional structure of membrane proteins (*1*). In the two-step model of membrane protein folding, individual helices are formed first, which then associate to form the complete protein (*2*, *3*). More recently, a more detailed four-step thermodynamic conceptual model of membrane protein folding has been proposed: (i) partitioning of the polypeptide between membrane and aqueous phase, (ii) folding of secondary structure elements, typically helices, (iii) insertion of the polypeptide into the membrane, and (iv) association of helices to form the complete protein (*1*). These steps can proceed along an interfacial path, a water path, or a combination of both. To study some of the conceptual steps in this mechanism, Wimley et al. have studied the partitioning of a series of host−guest pentapeptides (acetyl-WL-X-LL, with X being any of the 20 natural amino acids) in water/octanol and in a POPC[1] bilayer (*4*−*6*). They created an interfacial hydrophobicity scale based on the transfer free energy from water to octanol or the lipid bilayer interface, which has proved to be useful for the prediction of transmembrane segments in membrane proteins. The unfolded peptides are presumed to partition in the interface in the lipid bilayer systems, without deep penetration in the hydrocarbon core because of the lack of hydrogen bonding partners for the peptide backbone (*6*). Two of the host−guest pentapeptides (X = Arg or Lys) appear to form salt-bridge interactions between the charged side chain and the carboxyl group at the C-terminus, in octanol but not in solution (*5*). In octanol, the salt-bridge interaction in the Arg- and Lys-peptides causes a free energy reduction of 4 kcal/mol relative to a noninteracting charge pair. A similar trend is observed in the lipid bilayer for these peptides, suggesting the presence of a favorable electrostatic interaction (*5*, *6*). When the C-terminus of the peptide is protected, this interaction disappears, which suggests it was a salt bridge (*5*, *6*). In this paper, we use computer simulations to investigate these two peptides in different environments to help interpret these experiments.

Kessel and Ben-Tal have described the different contributions to the free energy of peptide−membrane association and reviewed computational methods for evaluating their magnitude at the mean-field level (*7*). They classified peptides into three categories depending on their location in the membrane. The first category includes peptides that

† This work was supported by the National Science and Engineering Research Council of Canada. D.P.T. is a Scholar of the Alberta Heritage Foundation for Medical Research. J.L.M. is supported by studentships from NSERC and Alberta Ingenuity.

* Corresponding author. E-mail: tieleman@ucalgary.ca. Fax: (403) 289-9311.

[1] Abbreviations: MD, molecular dynamics; POPC, palmitoyloleoylphosphatidylcholine; DOPC, dioleoylphosphatidylcholine; RMSF, root-mean-square fluctuation; RMSD, root-mean-square deviation; RDF, radial distribution function.

10.1021/bi027001j CCC: $25.00
Published on Web 07/11/2003

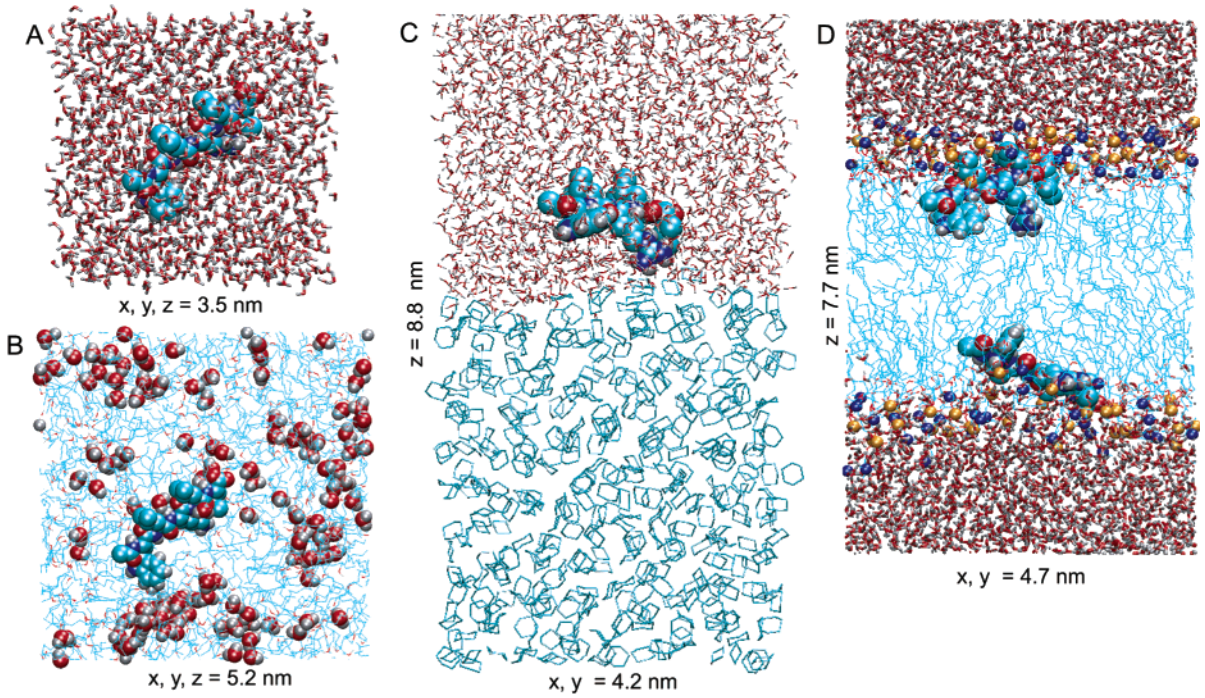

FIGURE 1: Overview of the four simulation systems, with the dimensions of the box. Starting configurations: (A) water, (B) water-saturated octanol (water molecules are shown in space filling form), (C) water/cyclohexane biphasic cell, and (D) a solvated lipid bilayer (phosphorus atoms are shown in orange and nitrogen atoms in blue). The peptides are shown in space filling form.

interact only with the hydrocarbon core, in which the energetics are dominated by the interaction between the hydrophobic transmembrane segments and the lipid tails. The second category consists of peptides that interact predominantly with the polar headgroup region; their energetics depends on the polar headgroups (mainly electrostatics) and specific peptide−lipid interactions. This category includes many peripheral membrane proteins. The last category corresponds to peptides that interact with both the headgroup and the hydrocarbon region of the lipid bilayer. Importantly, this class includes fusion peptides and anti-microbial peptides. The peptides studied in this paper have characteristics of both classes 2 and 3. The theoretical treatment of this type of peptide is substantially more difficult. The success of mean-field based computational methods depends on sufficient experimental data on the structure of the peptides and the nature of their interactions with the lipid bilayer. Their main advantage is the ability to describe both thermodynamic and long-term kinetic aspects of membrane−peptide interactions. Their main disadvantage is the lack of atomic detail in the description of the bilayer and the lack of internal degrees of freedom in the peptide.

Molecular dynamics (MD) simulations have become an established tool to study the structure and dynamics of biomolecules, complementary to experimental techniques and other theoretical methods (*8*, *9*). Increasing computer power and improved algorithms have enabled the study of larger systems on a time scale of up to about 100 ns, bringing a variety of more complex biological systems and processes within the reach of simulation. In particular, there has been a rapid development in the past few years of simulations of lipid bilayers and membrane proteins (*10*−*12*). Membrane peptides have been studied at simple interfaces (e.g., refs *13*−*15*) and in lipid bilayer interfaces (e.g., ref *16*). In a recent study, we showed how two anti-microbial peptides starting from outside the bilayer entered the bilayer and bound at well-defined positions (*17*).

In this paper, we describe molecular dynamics simulations of two pentapeptides (Ace-WLRLL and Ace-WLKLL) in water and three-membrane mimetic systems: (i) a water/cyclohexane biphasic cell, (ii) water-saturated octanol, and (iii) a solvated DOPC bilayer. We will address four questions that arise when considering the process of partitioning and insertion of these model peptides: (i) what structures do these peptides adopt in the different environments? (ii) What is the location of these peptides? (iii) What structural changes occur in the environment because of the peptides (*4*−*6*)? (iv) What is the behavior of tryptophan residues in the lipid−water interface region (*18*)?

To address the first question, we analyze backbone dihedral angles, the flexibility of the side chains in different environments, and use cluster analysis to investigate which conformations are dominant in each environment and monitor the formation of salt bridges and cation−π interactions. To answer the second and third questions, we study the change in the water−octanol structure induced by the peptides and the structural changes in the lipid bilayer/water interface. To address the fourth question, we analyze in detail the orientation of the Trp residue in the pentapeptides and its interactions with other side chains and lipids.

MATERIALS AND METHODS

Simulation Setup. Figure 1 summarizes graphically the different simulation systems. In each case, the peptides were initially built in an extended conformation. The arginine and lysine residues were protonated, while the C-terminus was deprotonated, yielding a net charge of zero for the peptide.

Peptide in Water. The peptide/water systems are cubic boxes of dimensions 3.5 × 3.5 × 3.5 nm; the Arg-peptide/water system consists of one peptide and 1371 water

molecules (4182 atoms), and the Lys-peptide/water system consists of one peptide and 1373 water molecules (4184 atoms).

Peptide in Water−Cyclohexane Biphasic Cell. A pre-equilibrated (10 ns) water−cyclohexane system was made in a rectangular box of dimensions 4.2 × 4.2 × 8.8 nm (Figure 1C). The water/cyclohexane interface, defined as the region where the water density drops from 90 to 10%, has a width of 0.7 nm. We placed the peptide in the water phase, ca. 1.5 nm above the center of the interface (Figure 1C). Water molecules that overlapped with the peptide were removed, and the system was energy-minimized. After 300 ps, the peptide was located at the interface with the Leu side chains inserted in the cyclohexane and the charged residues in the water phase. The Arg-peptide water/cyclohexane system contains one peptide, 434 cyclohexane molecules, and 2043 water molecules (8802 atoms in total), and the Lys system contains one peptide, 434 cyclohexane, and 2046 water molecules (8807 atoms in total).

Peptides in Water-Saturated Octanol. Each peptide was inserted into a preequilibrated (25 ns) cubic box of water-saturated octanol measuring 5.2 nm per side (*19*). All molecules that overlapped with the peptide were removed, resulting in the deletion of several octanol molecules per system. Several additional water molecules were deleted to bring the system to a mole fraction of water of 0.20. The Arg-peptide water/octanol system contains one peptide, 497 octanol molecules, and 129 water molecules (5426 atoms in total). The Lys system contains one peptide, 493 octanol molecules, and 128 water molecules (5379 atoms in total).

Peptides in a Solvated-Lipid Bilayer. The peptides were embedded in a preequilibrated (25 ns) lipid bilayer consisting of 64 molecules of DOPC (32 per leaflet). This DOPC structure is available from http://moose.bio.ucalgary.ca. Holes were generated in both sides of the lipid interface, at a location approximately suggested by the experimental data, by applying a radial force in a short MD simulation. The two peptides were then inserted into the resulting free space (*20*). The systems were resolvated with 43 water molecules per lipid and then energy minimized. The two peptides have different orientations in the interface, thus providing an internal control for convergence of the bilayer simulations. We will refer to the two peptides as upper and lower on the basis of their *z* coordinates in the simulation, but there is no fundamental difference between the two, and both should give the same results if our sampling would be complete. The Arg/bilayer system contains two peptides, 64 DOPC, and 2805 water molecules (12 009 atoms). The Lys-peptide/bilayer system contains two peptides, 64 DOPC, and 2807 (12 007 atoms). The initial dimensions of the systems are 4.8 × 4.6 × 7.9 nm.

Simulation Procedure. MD simulations were carried out using periodic boundary conditions with constant pressure and temperature. Except for the phospholipids and the charges on the octanol, we used the GROMOS96 43a2 force field (*21*) as implemented in the GROMACS software package (*22*−*24*). The octanol parameters were taken from ref *19* and the lipid parameters from Berger et al. (*25*). The water model used was SPC (*26*). Simulations were run with a 2-fs time step (5-fs time step for the lipid bilayer systems). Bond lengths were constrained using the LINCS algorithm (*27*). Lennard−Jones interactions were calculated with a 0.9/1.4 nm twin-range cutoff. The short-range electrostatic interactions were calculated to 0.9 nm, and the Particle Mesh Ewald algorithm was used for the long-range interactions (*28*). The neighbor list was updated every 10 steps. Each component of the systems (i.e., peptide, water, octanol, cyclohexane, and lipids) was coupled separately to a temperature bath at 300 K, using a Berendsen thermostat (*29*), with a coupling constant $\tau_T = 0.1$ ps. In the water and water/octanol simulations, the pressure was kept at 1.0 bar using isotropic pressure coupling (*29*) with $\tau_P = 1.0$. In the water/cyclohexane simulation, the *x* and *y* dimensions (the area of the interface) of the system were held fixed, while the *z* dimension was coupled to a pressure of 1.0 bar. The lipid bilayer MD simulations were performed with anisotropic pressure coupling, to 1 bar independently in *x*, *y*, and *z*, which allows the area per lipid to fluctuate. The time step was 5 fs for the lipid bilayer systems using a special treatment of the hydrogens in the peptide and the aromatic Trp ring (*30*).

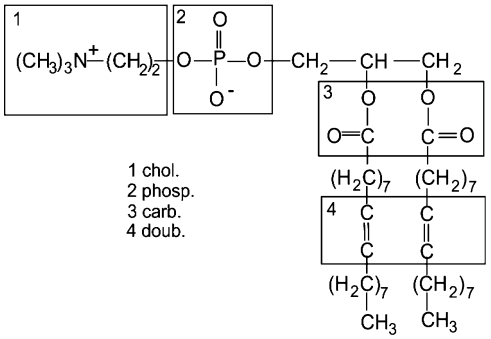

FIGURE 2: Schematic representation of the DOPC, with the name and structures of the groups used in the analyses.

Analyses. All analyses were done with GROMACS programs. Molecular graphics were made using VMD (*31*). The structure and definition of the groups used for analysis of the DOPC density profiles is shown in Figure 2.

Salt-bridge interactions were analyzed using two distances: D_{SC} is defined as the distance between the center of mass of the guanidinium or ammonium group and the center of mass of the carboxyl terminus of Leu5. We used 0.5 nm as the distance criterion for a salt bridge according to this definition. D_{SB} is defined as the minimum distance between any atom of the ammonium (Lys) or guanidinium (Arg) moiety and any oxygen atom of the carboxyl terminus. For the cation−π interaction (Figure 11), a distance $D_{C-\pi}$ was defined as the distance between the geometrical centers of the guanidinium and indole groups. The angle γ was defined as the angle between the normal vector on the plane of the guanidinium and the normal vector on the tryptophan ring. Cation−π interactions have two main conformations: stacked, in which the planes of the aromatic group and the planar cation are parallel, and T-shaped, where the planes are perpendicular. The γ angle will fluctuate between 0 and 45 and 135−180° in the stacked conformation and between 45 and 135° in the T-shaped conformation (*32*). Cluster analyses were based on a RMSD criterion of 0.12 nm for backbone plus C-β, following the algorithm of Daura et al. (*33*).

RESULTS

Peptide Conformation. Figure 3 gives an impression of the peptides in different environments, toward the end of

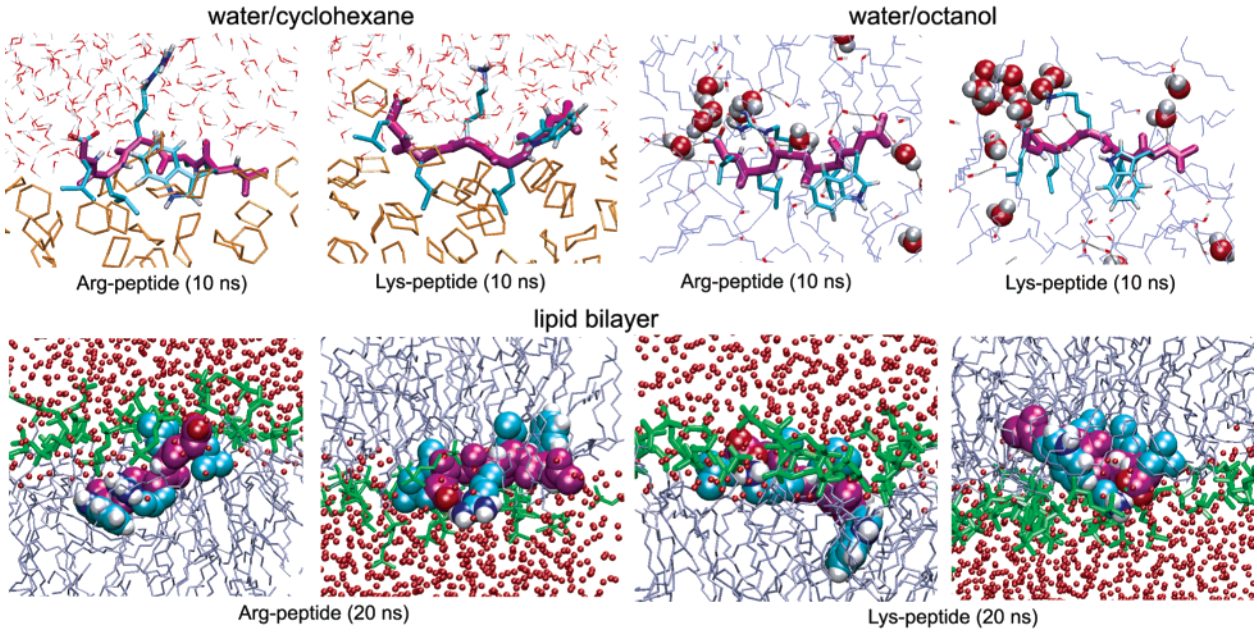

FIGURE 3: Snapshots of both peptides in water/cyclohexane, octanol, and lipid bilayer. The peptide backbone is violet, and the side chains are blue. In the octanol system, water molecules are shown as space filling. In the lipid bilayer snapshots, the whole peptide is space filling with the oxygen of the carboxy-terminus in red, the hydrogens in the lysine and arginine side chains white, and the nitrogens dark blue. The lipid headgroups are shown as thick green bonds, the chains as thin bonds, and the water as small red spheres.

Table 1: Percentage of the Total Population for the First Five Clusters of the Peptides in Each of the Different Environments, by Clustering Based on a Root-Mean-Square Deviation in Structure of 0.12 nm

	water		water/cyclohexane		octanol		lipid bilayer	
cluster	Arg	Lys	Arg	Lys	Arg	Lys	Arg	Lys
1	33.7	26.3	55.0	56.8	35.0	71.8	49.0	50.6
2	10.1	17.1	9.6	10.6	30.2	13.0	38.5	35.6
3	9.8	8.3	6.2	7.7	11.3	11.7	7.0	8.2
4	6.0	7.7	5.5	5.0	9.9	1.6	4.2	2.2
5	4.6	6.0	4.5	3.6	6.0	1.1	0.7	1.6
TP[a]	64.2	65.4	80.8	83.7	92.4	99.2	99.4	98.2

[a] TP is the sum of the first five clusters.

each simulation. To analyze the range of conformations in the different environments, we used cluster analysis based on the backbone plus C-β carbons of the peptide (Table 1). The largest number of clusters occurs in water, whereas in the lipid bilayer and in octanol the three or four largest clusters account for more than 90% of the conformations.

Figure 4 shows the different conformations in the clusters. In all cases, mostly extended conformations dominate. The main differences are in the backbone dihedral angles of the Leu2 and Leu4 residues. The effect of the environment on the mobility of the peptides is also of interest, in addition to its effect on the structures. Figure 5 shows the root-mean-square fluctuation (RMSF) for each residue in all four environments, which is a measure of their mobility.

In water, the backbone dihedrals angles of the Arg-peptide remain in the β-region of the Ramachandran plot with considerable fluctuations of approximately 30°. In the Lys-peptide, the residues Leu2 and Leu4 show multiple transitions between the β- and the α-region. The flexibility of the side chains is most pronounced in water. The largest RMSF in the Arg-peptide corresponds to the Arg side chain, whereas in the Lys-peptide the N-terminus (Ace-Trp1-Leu2) is most flexible.

In water/cyclohexane, the backbone dihedral angles are comparable to those in water, except for the extended conformation of Leu2. As in water, the Leu4 side chain shows either a completely extended backbone or a kinked conformation. The highest RMSF values correspond to side chains facing the water phase, whereas the lowest fluctuations are found for residues interacting with the cyclohexane. The Arg-peptide has a salt-bridge interaction for 2 ns (between 6 and 8 ns). The Lys-peptide mostly has a kinked conformation that favors the salt-bridge interaction, but exposed to water this salt bridge is not very stable. The Trp1 ring in both peptides is usually located in the interface, either perpendicular or parallel to the interface with occasional excursions into the water or cyclohexane phase.

In octanol, the Lys-peptide forms a stable salt bridge and remains in approximately the same conformation throughout the simulation. The backbone dihedral angles of Leu4 fall within the α-helix region of the Ramachandran plot. The Arg-peptide shows significant fluctuation between a salt bridge and a cation$-\pi$ interaction, but the salt-bridge interaction is predominant. As the peptide switches between the two interactions, the backbone dihedral angles of Leu4 switch between the β-extended and the α-helix region of the Ramachandran plot. The flexibility of the side chains of the Arg-peptide, especially for Trp1, Arg3, and Leu5 is comparable to the peptide in water.

In the DOPC bilayer, the peptides remain in the interface area of the lipid bilayer throughout the simulations (Figure 6). The Arg-peptides show two different dominant interactions: the upper peptide has a cation$-\pi$ interaction between the Trp and the Arg side chains; the lower peptide forms an intramolecular salt bridge. In contrast, the Lys-peptides have only the salt-bridge interaction. The values for the backbone dihedral angles for both Arg- and Lys-peptides are comparable to those in the other environments. Leu4 adopts only one conformation in both Lys-peptides, fixed by the intramolecular interaction. In the Arg-peptides, the dihedral

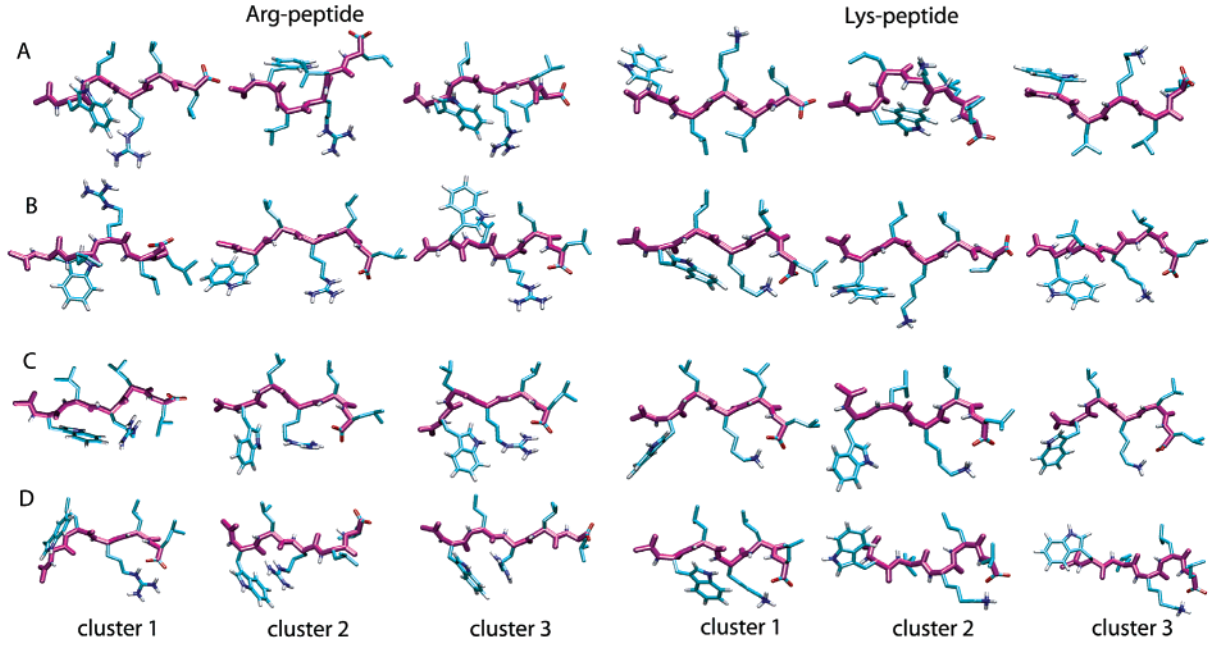

FIGURE 4: Representative snapshots from the three largest clusters for both the Arg- and the Lys-peptides. (A) water, (B) water-cyclohexane, (C) octanol, and (D) lipid bilayer.

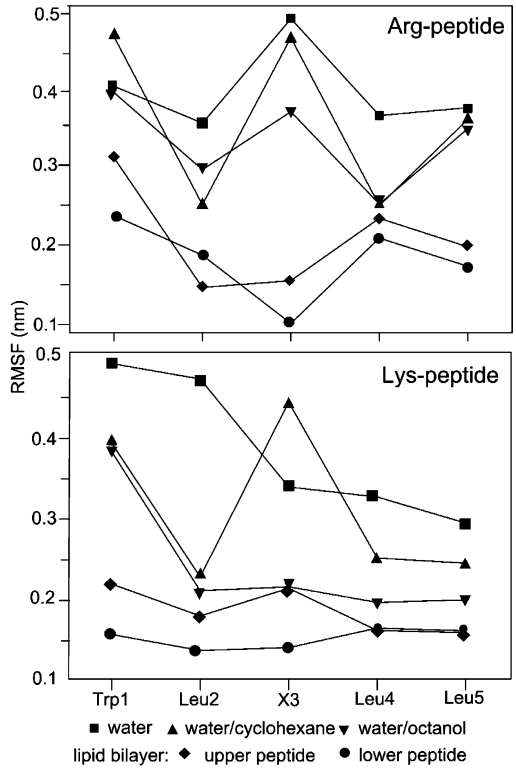

FIGURE 5: RMSF of the peptides in different environments. The RMSF for each residue was averaged over all side chain atoms.

angles of Leu4 of the upper peptide lie in the β-region of the Ramachandran plot, and the dihedral angles of the lower peptide lie in the α-helix region. The cation$-\pi$ interaction in the Arg-peptide strongly limits the flexibility of the Trp and Arg side chains. When both groups are involved in this interaction, the RMSF values are minimal; Trp has an average RMSF of 0.086 nm, Arg is 0.066 nm over the first 15 ns; but when the interaction is broken, the side chain flexibility increases to values of 0.30 nm for Trp and 0.19 nm for Arg. The mobility also depends on the orientation in the membrane; as a salt-bridged peptide moves from a perpendicular to a parallel orientation with respect to the membrane, the RMSF decreases from an average 0.30 nm over the first 10 ns to 0.16 nm over the last 10 ns. The Lys-peptides both form a salt bridge, but the side chains of the upper peptide initially are more flexible than those of the lower because of its different location and orientation in the bilayer. The upper peptide has a perpendicular orientation with respect to the interface in the first 15 ns and then becomes parallel, whereas the lower peptide remains in a parallel orientation throughout the simulation, suggesting this is its primary orientation.

Distribution of the Peptides in Octanol and the Lipid Bilayer. The water-saturated octanol system has no well-defined interface but consists of a complex mixture of hydrophobic and hydrophilic regions (*19*, *34*, *35*). A cluster of water molecules surrounds the charged residues, while the rest of the peptide is surrounded by hydrophobic octanol tails. To analyze the effects of the peptide on the structure of the water−octanol systems, we calculated the radial distribution function (RDF) of water oxygen atoms and octanol oxygens around each of the peptide side chains for the first 2 ns and the last 2 ns (data not shown). Leu2 and Leu4 in both the Arg- and Lys-peptide are surrounded by hydrophobic tails, and the RDFs do not change during the simulation. Initially, the Trp side chain in both peptides is located near a cluster of water molecules (Figure 1B), but after 4 ns this is no longer the case, and for the remainder of the simulation the Trp side chain is surrounded only by hydrophobic chains. In the Arg-peptide, the number of water molecules surrounding the side chain remains constant at 8−10. In the Lys-peptide, the Lys side chain was initially placed in a hydrophobic region, so that over the course of the simulation the number of water molecules increases from 0 to 8−10, comparable to Arg. The RDF for the Lys side chain with the water oxygen shows an increase of the peak present at below 0.5 nm until 6−8 ns time, then remains constant. The salt bridge is formed in the first picoseconds of the simulation time. In both cases, the water/octanol forms

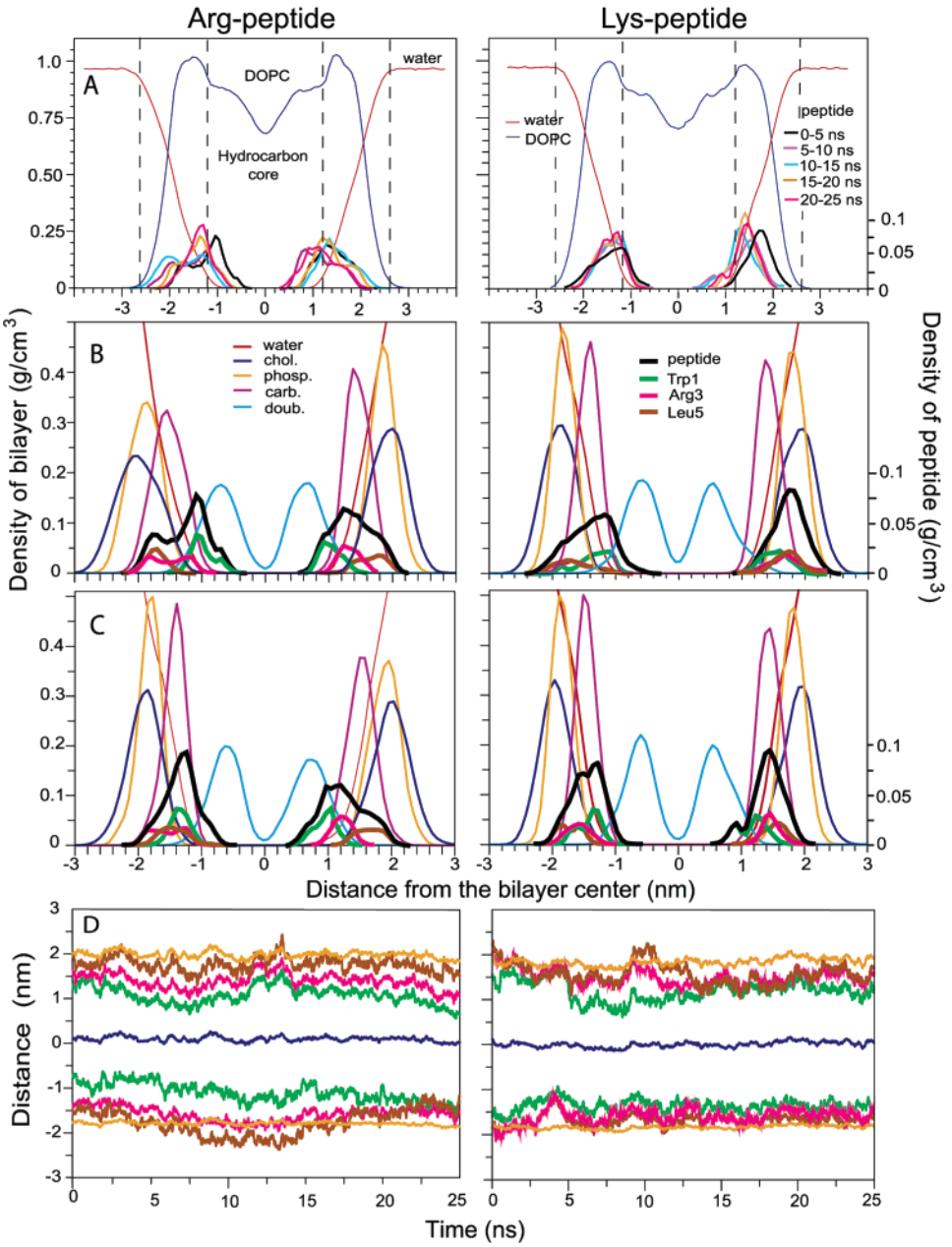

FIGURE 6: Density profiles along the bilayer normal. Left column: Arg-peptide and right column: Lys-peptide. (A) Density profiles of the peptides averaged over 5 ns segments of the trajectory; the dashed lines represent the interface zone of the lipid bilayer. Water and lipid density profiles are averaged over 25 ns. Density profile of the peptides (B) averaged over the first 5 ns and (C) averaged over the last 5 ns of simulation; the scale of the left and right of the graphs corresponds to the lipid components and the peptide and/or side chain, respectively. Profiles in panels B and C are showing the density of the bilayer interface components (as choline, phosphate, and carbonyl) and one component of the hydrocarbon core of the bilayer, the double bond distribution. These different groups are defined in Figure 2. Also shown are the distributions of the side chain residues (Trp1, Arg or Lys, and Leu5). (D) The *z* coordinate for the center of mass of phosphate groups, the side chain of Trp1, Arg3 or Lys3, and Leu5 with respect to the center of mass of the lipid bilayer.

a hydration shell surrounding the salt bridge, creating a network of hydrogen bonds between water, octanol, and the side chains (details not shown).

Figure 6 shows the density profiles of the peptides in the lipid bilayer systems. Figure 6D shows the *z* coordinate of the center of mass of the side chains Trp1, X3, and Leu5 with respect to the center of mass of the lipid bilayer. The peptides remain in the lipid bilayer interface throughout the simulations. The Arg-peptide shows larger fluctuations in its position in the lipid bilayer as compared to the Lys-peptides and deeper insertion into the hydrocarbon core of the bilayer. The density profile for the choline, phosphate, carbonyl, and double bond groups averaged over the first and last 5 ns of the simulations shows the location of the peptides in more detail (see Figures 6B,C and 2 for the group definitions). In both peptides, Trp1 penetrates deeply in the hydrocarbon core of the lipid bilayer, while Arg3 or Lys3 and Leu5 remain in the interface area.

The upper Arg-peptide (the one forming the cation$-\pi$ interaction) remains in a perpendicular orientation with respect to the interface throughout the simulation (Figure 6D). The Trp remains between the double bond and the carbonyl area of the lipid bilayer, while the side chains of Arg3 and Leu5 remain near the lipid carbonyl groups. In this orientation, the lipid headgroups are practically unperturbed. The superimposed structures for the upper peptide

show mainly fluctuations in the C-terminus, which is located near the lipid phosphate groups and is water-exposed. In the lower Arg-peptide (forming the salt bridge), the orientation and the position in the lipid bilayer changed during the simulation. In the first 17 ns, the peptide has a perpendicular orientation with respect to the interface area, and the position of the peptide fluctuated in the interface (Figure 6D). The C-terminus moves outside of the interface for approximately 7 ns, to re-enter again at the interface. The Trp1 side chain penetrates deeply in the hydrocarbon core region, similar to the location of the Trp side chain in the upper peptide at approximately 1 nm from the center of the lipid. The reinsertion of the C-terminus in the interface is initiated by a transition in the peptide orientation. In the last 5 ns of the simulation the peptide has a parallel orientation, and the peptide overlaps with the lipid carbonyl distribution. The change in the orientation of the peptide compresses the profiles of the choline, phosphate, glycerol (not shown in the graphs), and carbonyl groups.

In the Lys-peptides, as discussed above, the upper peptide appears more flexible than the lower because in the first 12 ns of the simulation a significant part of the peptide (C-terminus) is located in the water phase. After 12.5 ns, the peptide orientation becomes parallel to the lipid interface. However, the lower peptide always has the same orientation along the simulation. In the last 10 ns of the simulations, both peptides have the same relative location and orientation in the interface, in the carbonyl area of the lipids.

Orientation of Trp Residues in the Lipid Bilayer. The orientation of Trp residues can be described by two order parameters, S_N and S_L (Figure 2 of ref *36*). S_N describes the angle between the normal to the lipid bilayer plane (the *z* axis) and a normal vector on the plane of the aromatic ring. S_N has two extremes values: -0.5 means this vector is perpendicular to the *z* axis; thus, the ring itself is perpendicular to the membrane plane. A value of 1 means this vector is parallel to the *z* axis; thus, the ring itself is parallel to the membrane plane. S_L describes the angle between the *z* axis and a vector from the Cg to Ch2 in the Trp residue. If S_L is 1, the long axis of the side chain is parallel to the *z* axis and S_N can only be -0.5, perpendicular to the *z* axis. If S_L is -0.5, the long axis is perpendicular to the *z* axis, S_N has a value of 1, and the plane of the ring is parallel to the membrane. If S_L goes from -0.5 to 1, S_N can assume almost the entire range of values (from -0.5 to 1) by rotation around the long axis. These order parameters are shown in Figure 7.

During the first 15 ns (cation$-\pi$ interaction), the upper Arg-peptide remains in a parallel orientation with respect to the plane of the membrane (S_L value -0.5), with fluctuations in S_N that correspond to rotation around the long axis (Figure 7A). During this time, the Trp ring interacts with the guanidinium group, which restricts the possible conformations. As the distance between the groups increased, the Trp changed its orientation from a parallel to an almost perpendicular orientation (S_L values nearly 1 and S_N -0.5). In the Arg-peptide involved in the salt bridge, the orientation of the Trp ring remains perpendicular to the plane of the membrane for the first 20 ns, with values of the S_L nearly 1 and S_N -0.5 (Figure 7B). After 20 ns, the orientation of the aromatic side chain starts to change from perpendicular to parallel to the interface, tracking the change in orientation

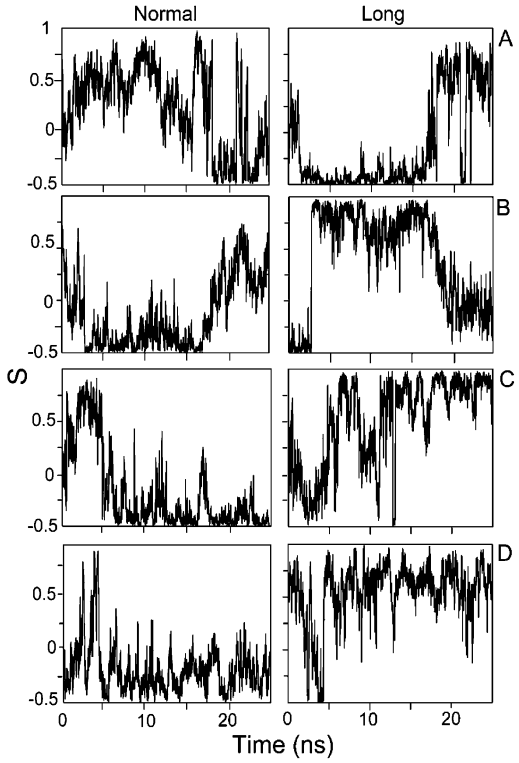

FIGURE 7: Orientations of the Trp1 ring in the lipid bilayer simulations, as a function of the time, defined by S_N (left column) and S_L (right column) (see text). Arg-peptide: (A) upper and (B) lower peptide. Lys-peptide: (C) upper and (D) lower peptide.

of the peptide backbone perpendicular to parallel (see Figure 6D). The change in the orientation of the tryptophan ring also is influenced by the location of the peptide in the lipid bilayer. In the first 20 ns, the Trp ring lies between the lipid carbonyl group and the upper part of the hydrocarbon tails. When the change in the orientation of the peptide is accomplished, the Trp lies in the carbonyl area of the lipid bilayer, oriented parallel to the lipid/water interface. The Trp residues in both Lys-peptides have similar orientations (Figure 7C,D), in agreement with their similar depth and overall orientation in the bilayer.

To study the potential interactions of the Trp side chain with the lipid headgroups, we analyzed two parameters: (i) the minimum distance between the Trp ring and the choline group of the lipids (data not shown) and (ii) the RDF for the choline group with respect to the center of the Trp ring. The RDFs over the last 15 ns are shown in Figure 8. When the Trp lies in the carbonyl area of the lipid bilayer (i.e., for the lower Arg-peptide and for both Lys-peptides), the distance between both groups has a range between 0.45 and 0.60 nm. These small distances allow the formation of cation$-\pi$ interactions between the peptide and the lipid headgroup.

A snapshot showing the interaction between the Trp-ring and the headgroup of the lipids is shown in Figure 9. The upper Arg-peptide that forms the intramolecular cation$-\pi$ interaction does not display any peak near 0.5 nm—the first peak is at 1.0 nm, but in the last 5 ns when the interaction is broken, the RDF profiles shifted to shorter distance, and the peak changed to 0.7$-$0.8 nm. The lower Arg-peptide over the last 15 ns of simulation shows a shift in the position of the first peak from 0.50 to 0.45 nm. The Lys-peptides

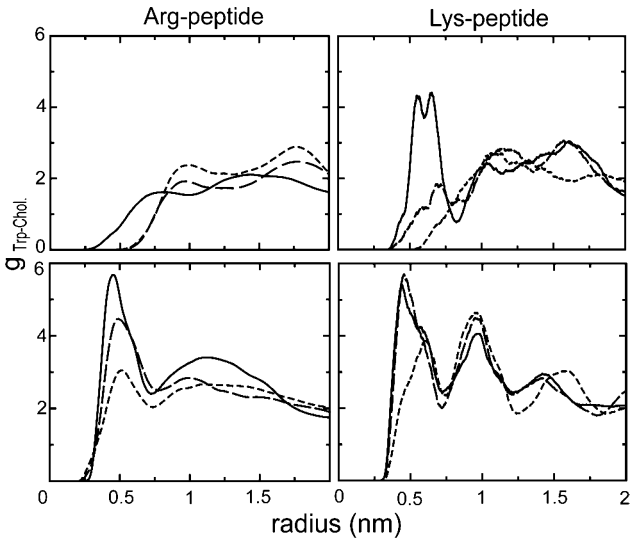

FIGURE 8: Radial distribution functions $g_{Trp-Chol}$ for the simulations in the lipid bilayer. First row upper peptide and second row lower peptide. The average is between: 10−15 ns (short dashed lines), 15−20 ns (long dashed lines), and 20−25 ns (black line).

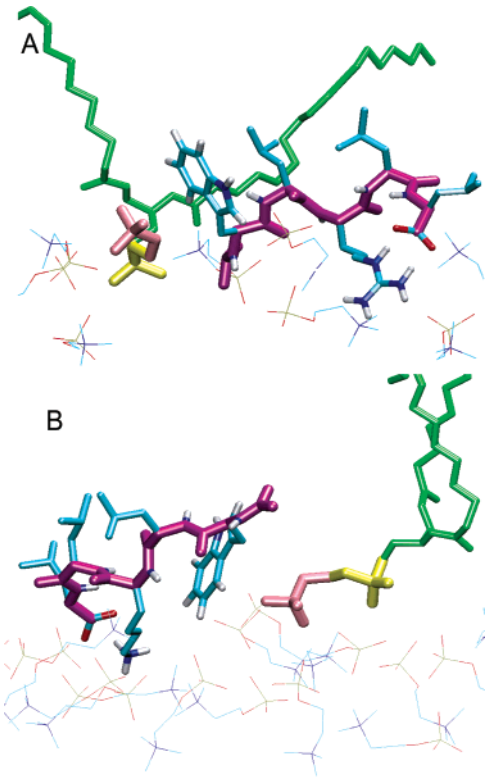

FIGURE 9: Snapshots of the interaction in the lipid bilayer between the Trp side chain and the choline group. (A) Lower Arg-peptide and (B) Lys-peptide. The peptide backbone is shown in violet, the choline group is pink, the phosphate group is yellow, and the rest of the lipids are displayed in green.

behave similarly to the Arg-peptides. The RDF from 10 to 15 ns of the upper Lys-peptide does not show any cation−π interaction between the peptide and the lipid, and the profiles are similar to the upper Arg-peptide. Between 15 and 20 ns, during which the peptide has a parallel orientation and is located in the carbonyl area, the RDF shows a maximum in the first peak at 0.5 nm. After 20 ns, the Trp penetrated deeper in the hydrocarbon core, the peaks in the RDF moved to 0.6 nm, and the interaction was broken. In the lower Lys-peptide, even in the early stage of the simulations, the RDF shows a maximum at 0.6 nm, and at the end of the simulation the peaks shifted to 0.45 nm.

Salt-Bridge Formation. As described in the Materials and Methods, we use two distances to analyze salt bridges. D_{SB} is the minimum distance between any two atoms in the interacting side chains, and D_{SC} is the distance between the two groups. In Figure 10, both distances as well as the distribution of D_{SB} are shown for the peptides in the membrane mimetic systems.

The salt-bridge interaction is not formed in water. In water/cyclohexane, the salt bridge is observed only sporadically for a few picoseconds, consistent with estimates of the marginal stability of salt bridges exposed to water (*37*).

In octanol, salt bridges are formed in the first picoseconds of the simulations. In the Lys-peptides, the salt bridge is stable throughout the simulation. The distribution of D_{SB} has a strong maximum at 0.20 nm; the distance remains below 0.5 nm, and the D_{SC} distance has an average of 0.3 nm. In the Arg-peptides, the interaction is present in the first 6 ns of the simulation, but in the last 4 ns of the simulation the salt bridge is broken. The distance distribution for the Arg-peptide shows a maximum at 0.25 nm and a narrower distribution than in water/cyclohexane, between 0.15 and 0.75 nm. However, the D_{SC} distance remains above 0.5 nm. Occasionally, close contacts occur between the Arg side chain and the Trp ring. To analyze if cation−π interactions between Arg and Trp were likely in water/octanol and to further investigate the stability of the salt-bridge interaction, we performed two additional 10 ns simulations in water−octanol: one with the cation−π interaction and one with the salt-bridge interaction already formed. The cation−π interaction is not stable in the first simulation, and instead a salt bridge is formed after 8 ns. The salt bridge in the second simulation remains stable over 10 ns.

In the lipid bilayer, both Lys-peptides form stable salt-bridge interactions. The distance D_{SB} remains below 0.2 nm, and D_{SC} has an average of 0.4 nm. In the upper peptide, the salt bridge is broken temporarily between 8 and 12 ns, when the C-terminus of the peptide moved outside of the lipid bilayer, but reformed quickly after the C-terminus reinserted into the lipid bilayer. In the Arg-peptides, the lower peptide shows the salt-bridge interaction during the entire simulation, with D_{SB} below 0.2 nm and D_{SC} at an average of 0.4 nm. The upper peptide forms a cation−π interaction that will be discussed in the next section.

Cation−π Interactions. A cation−π interaction as defined in the Materials and Methods occurs for only 0.5 ns in the Arg-peptide in the water/cyclohexane systems. As mentioned above, stable cation−π interactions do not occur in water/octanol. In the lipid bilayer systems, however, the interaction is present in the upper Arg-peptide for the first 15 ns of the simulation, with an average distance of 0.4 nm (Figure 11A) and a small approach angle γ. This is consistent with the statistical analysis of Minoux and Chipot who found that cation−π interactions involving arginine most frequently occur in the stacking conformations in soluble proteins (*38*).

DISCUSSION

Peptide Structure. Our first objective was to determine the conformations of the peptides in the membrane mimetic

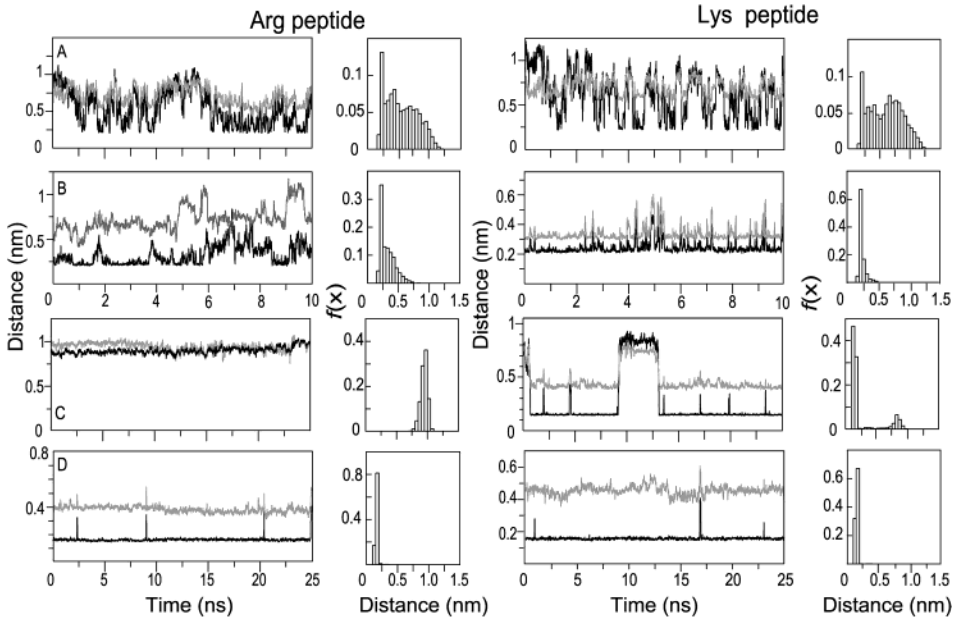

FIGURE 10: Salt-bridge interactions in the peptides in the four simulation systems: the distances D_{SC} (gray lines) and D_{SB} (black lines) as function of time and as histograms (D_{SB} only). (A) Water/cyclohexane and (B) water/octanol (10 ns of simulation). Lipid bilayer: (C) upper peptide and (D) lower peptides (25 ns of simulation).

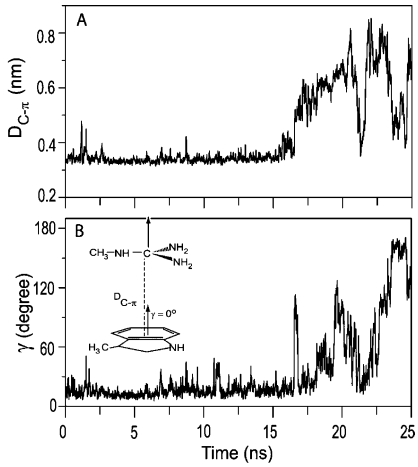

FIGURE 11: Analysis of the cation$-\pi$ interaction (see Materials and Methods) for the upper Arg-peptide at the lipid/water interface. (A) $D_{C-\pi}$ distances and (B) γ angle as a function of time. The inset shows the definition of the distance $D_{C-\pi}$ and the angle γ used in the analysis.

systems—water−octanol, water−cyclohexane, and a phospholipid bilayer—and the location of the peptide in the bilayer, neither of which is readily experimentally accessible. These peptides were designed to have no secondary structure in solution to make it possible to determine the free energy of transfer of an unfolded polypeptide chain from solution to membrane. Indeed, CD spectroscopy shows they adopt random coil conformations in both water and water-saturated octanol (*4*, *5*). These experiments, however, do not preclude the possibility of different conformations in different environments (*5*, *6*). In all systems, the peptides adopt mostly extended conformations, but there are two major conformational families. The principal difference is in the backbone dihedral angles of Leu4 and Leu5. One major family consists of completely extended structures in water, whereas the second major family consists of structures with a kink at the C-terminus. The shift between the two conformations is mainly due to strong intramolecular interactions in more hydrophobic environments: for both the Lys- and the Arg-peptide, salt bridges are found in octanol, in agreement with the experimental evidence (*5*, *6*). We found two electrostatic interactions in the lipid bilayer: either a salt bridge or a cation$-\pi$ interaction. Both of these, once formed, are stable over extended periods of time, which makes it hard to determine which is more favorable. Nonetheless, the cation$-\pi$ interaction is broken after 15 ns in the lipid bilayer and does not reform, suggesting this interaction is weaker than the salt bridge (Figure 11). This is consistent with experimental results, which show that the relatively high hydrophobicity of the Arg- and Lys-peptides is abolished if the C-terminus is capped in octanol, so that salt-bridge formation is no longer possible (*4*, *5*).

An interesting question is why only the Arg-peptide forms a cation$-\pi$ interaction in the lipid bilayer, while the Lys-peptide does not. In soluble proteins, both cationic side chains prefer to interact with the tryptophan side chain to the tyrosine and phenylalanine residues (*39*, *40*). An analysis of the residue frequency and pairing preferences at 621 protein−protein interfaces showed that the most frequent hydrophobic-charged side chain interaction occurs between the Trp ring and the Arg side chain in a stacking conformation (*41*). Adamian and Liang analyzed the helix−helix packing interaction of residues in 14 membrane proteins. They found that there is a high propensity for interhelical interactions between aromatic residues and basic residues (Arg−Trp, His−Trp, and Lys−Tyr), strongly suggesting cation$-\pi$ interactions play a role in membrane proteins. The residue pair propensities found were 2.5 for Arg with Trp, 0.4 with Phe, and 1.4 with Tyr. For Lys these numbers are 0.6 with Trp, 0.4 with Phe, and 2.5 with Tyr. These results suggest that an interaction between the Lys side chain and the Trp ring is less likely to be observed in membrane proteins (*42*). One reason for this might that the Arg side chain can still donate several hydrogen bonds while simultaneously interacting with an aromatic ring (if it is stacked), whereas lysine would be unable to both form hydrogen bonds and interact

with the aromatic ring (*39*). We analyzed the average number of hydrogen bonds between the Arg side chain and the water in the lipid bilayer system, normalized to the total number of hydrogen bonds that the Arg side chain could form. When the Arg side chain is interacting with the Trp ring, the normalized number of hydrogen bonds has a value of 0.32. When there is no interaction between these groups, the value increases to 0.42. This demonstrates that the Arg side chain can indeed form hydrogen bonds while also participating in a cation−π interaction. Although from the simulations it is not clear that this particular peptide forms cation−π interactions rather than salt bridges, and the experimental data suggest salt bridges are more favorable, it is nonetheless intriguing that this interaction is observed so prominently. A growing class of Trp and Arg rich short antimicrobial peptides might depend on this type of interaction for its activity (*43*).

There is an interesting difference in the distance D_{SB} between water−octanol and the lipid bilayer: in the bilayer, D_{SB} has average values of 0.20 nm whereas in octanol the average is 0.27 nm. This difference appears because of the environment where this interaction occurs. In water−octanol, water molecules and hydroxyl groups that act as a hydration sphere surround the peptides. The peptides in the lipid bilayer however are in a more hydrophobic environment, below the lipid headgroup and overlapping with the carbonyl area, where the salt bridge becomes stronger.

Peptide Location. In water/cyclohexane, the peptides are clearly located at the interface, as expected, and it only takes a few hundred picoseconds of simulation before they reach their average orientation. In the lipid bilayer, it takes tens of nanoseconds for the peptides to move to their preferred location in the bilayer, but this is clearly one interesting aspect of the current simulations. During the final part of the bilayer simulations the backbones of three out of four peptides are located in the carbonyl region of the lipids. The use of two peptides starting from two different orientations provides a control on convergence that a simulation of a single peptide cannot provide. Although the simulation of the Arg-peptide does not converge completely, both Lys-peptides and one of the Arg-peptides end up orientated parallel to the lipid−water interface and are located in the lipid carbonyl region. The location is consistent with experimental calorimetric and NMR data (*4*−*6*), but the simulations provide a more detailed view of the exact location and the interactions with the surrounding lipids.

Effect of the Peptides on Octanol and Lipid Structure. The third question we asked was the following: what is the effect of the peptides on the water−octanol and lipid bilayer structure? In water−octanol, the solvent rearranges to pack around the peptides, matching hydrophobic side chains with hydrophobic octanol tails. The peptides are nearly completely surrounded by hydrophobic tails, but the number of hydrogen bonds that stabilize the main chain in the peptides are comparable to the water−cyclohexane and the lipid bilayer systems. In the lipid bilayer, the results are somewhat subtler than in water/octanol. Depending on the orientation of the peptide, a significant change in the distribution of headgroup atoms is observed. The peptide appears to have two alternate extreme orientations, one parallel and one perpendicular to the interface, where the parallel one is more stable. When the peptides have a perpendicular orientation, the N-terminus is located deeper in the lipid bilayer; sometimes the Trp residues penetrated the hydrocarbon core sufficiently deeply to overlap with the double bond distribution of the lipid tail. The C-terminus is located within the headgroup region, and both the Arg- and the Lys-peptides move outside of the lipid−water interface for a few nanoseconds. The perpendicular orientation of the peptide has little effect on the density profiles of the lipid bilayer, but water molecules penetrate below the carbonyl area to form hydrogen bonds with the Trp side chain. When the peptide orientation is parallel to the interface, the peptides are located below the headgroup and overlap with the carbonyl area of the lipid. The choline and phosphate density profiles become sharper, and the phosphate−phosphate distance is somewhat less than in the pure bilayer. This change appears to be mainly due to the presence of the Trp side chain in the peptides, its cation−π interaction with the choline group, and the hydrogen bonds with the carbonyl groups and water.

Trp Interaction with the Lipid Bilayer. The exact reasons for the preference of the Trp side chain for membrane interfaces remain unclear. Yau et al. have studied the preference of indoles for lipid interfaces by NMR (*18*). This study showed that this preference is not due to hydrogen bonding or dipolar interactions and suggests the π-electronic structure and the associated quadrupolar moment of Trp and its geometrical shape might be dominant. Interestingly, recent experimental data suggest that the specific interhelical interactions between basic residues and Trp residues through a cation−π interaction may play an important role in the folding of membrane proteins (*44*). The difference in behavior of the Trp residue between simulations of octanol and phospholipid is that in octanol the imino group does not form hydrogen bonds. In the lipid bilayer for both peptides, cation−π interactions between the Trp ring and the choline groups of the lipid bilayer are observed. The cation−π interaction between lipids and Trp has a perpendicular geometry, in contrast to the stacked Arg−Trp interaction. This only involves one methyl of the choline group at close distance from the Trp ring. In addition to the cation−π interaction, the Trp side chain forms hydrogen bonds with the interfacial water and the ester carbonyl group of the lipids. Grossfield and Woolf studied the interaction of the tryptophan analogues (indole and *N*-methylindole) with POPC lipid bilayers by MD (*45*). The indole shows hydrogen bonding in the interfacial area of the lipids, and on average one of the four hydrogen bonds is between the imino group and the lipid groups. The energetically most favorable interactions appear to be when the analogues are located in the lipid headgroup region. In addition, the indole molecules appear to form hydrogen bonds when only 0.9 nm away from the center of the lipid bilayer. Our results also show that when the Trp is deeper in the hydrocarbon core (average of 1.0 nm from the bilayer center), it still forms between one and two hydrogen bonds to interfacial water.

Limitations of the Simulations. It is useful to consider the limitations of the simulations presented in this study. In the initial structure, the peptides have different orientations in the lipid bilayer. Despite the long simulation length by current standards, we do not see full convergence to a single family of conformations or a frequent transition between both families. The Lys-peptide shows two conformations; although they are rather similar and both include the salt bridge, they

differ in the backbone dihedral angles for Leu4. In the simulations, these peptides converged to a similar orientation and location in the lipid bilayer. In contrast, the Arg-peptides are a more complicated issue because they have two different intramolecular interactions (cation$-\pi$ interaction and salt bridge) that both are stable on the simulation time scale. On the basis of these simulations, it is not possible to estimate what simulation length would be required to determine which interaction is more favorable. Although perhaps in a simpler solvent (such as an octanol/water mixture) a free energy difference between the two could be calculated by, for example, umbrella sampling, this will likely remain infeasible in the membrane environment in the near future. It is possible that the free energy difference of these two conformations is sufficiently small that both occur, although experiment suggests that salt-bridge formation is the dominant factor because the unexpectedly high hydrophobicity disappears if the C-terminus is capped. Nonetheless, it is conceivable this changes other properties of the peptide, too. Sampling in water, water/cyclohexane, and water/octanol is much more complete.

A second concern is the accuracy of the force field used in the simulations. Two papers on force fields similar to the one used by us have shown that cation$-\pi$ interactions (*38*) and the interactions of aromatic rings with interfaces are reasonably well-represented (*46*). In addition, the parameters used in this study have been used in many previous studies of membrane proteins. Nonetheless, recent increases in computer power and efficiency of simulation algorithms now allows extensive parametrization of force fields on thermodynamic data, including free energies of hydration and partition coefficients (*47*−*49*). Use of such data in testing and reparametrizing some force field values could lead to considerable improvement toward quantitative agreement with experimental thermodynamic properties, such as the actual values of experimentally determined hydrophobicity scales. Our initial goal was to calculate relative free energies for the different pentapeptides to further assess the accuracy of the parameters, but the degree of sampling in the lipid bilayer systems is insufficient to obtain such results with statistical accuracy with current computational capabilities. The results of this paper however do show that many more qualitative properties can be obtained with current simulations. The simulations in octanol and water/cyclohexane also suggest that it might be possible, although computationally very expensive, to calculate the hydrophobicity scale in water/octanol as a test of simulation methods and force fields.

Implications for Membrane Protein Thermodynamics. In the four-step model, the insertion of the unfolded peptide corresponds to an early stage of the membrane protein folding mechanism, namely, the partitioning between the water and the water/lipid interface (*1*). Studying the partitioning is a difficult task, especially in the lipid bilayer membrane. In the simple water/cyclohexane, the partitioning of the peptide in the interface occurs rapidly, consistent with previous simulations (*13*, *15*, *50*). In the lipid bilayer, the insertion depends on the hydrophobic/hydrophilic character of the peptides, and the packing and disruption of the headgroup interactions, especially hydrogen bonds. The peptides in our study are too small to adopt a secondary structure. However, the unfolded structures of these peptides in membrane mimetic systems allow studying interactions that could stabilize an unfolded peptide along the interfacial path in the membrane protein folding process. The dominance of electrostatic interactions in these peptides suggests the importance of the interaction in the stabilization of an unfolded peptide in the lipid bilayer. After the partitioning of unfolded peptides in the membrane, the electrostatic interaction could stabilize the conformation of peptides and induce the formation of secondary structure in the protein. Although the Arg side chain shows a higher tendency than the Lys side chain to interact with the Trp side chain, both peptides are very comparable in their location in the bilayer and the importance of salt-bridge formation in determining their partitioning. This is consistent with the small difference in free energy of transfer from water to the lipid bilayer interface found experimentally: -0.88 ± 0.11 kcal/mol for Arg versus -0.99 ± 0.11 kcal/mol for Lys (*6*).

CONCLUSION

In the molecular dynamics simulations presented in this work, the partitioning of two model peptides (Ace-WL-X-LL, X= Arg or Lys) at different interfaces was studied. The results give insight into the location of these peptides in the bilayer, the effect of salt-bridge and cation$-\pi$ interactions on the conformation and partitioning of the peptides, the effect of the environment on peptide conformations, and the effect of the peptides on the structure of the environment.

The peptides have extended conformations in water and are flexible, but in hydrophobic environments salt bridges between Lys and Arg and the C-terminus limit the number of major conformations to just a few. This effect is strongest in the octanol and lipid bilayer environments. The salt bridges appear strongest in the bilayer, the most hydrophobic environment.

The simulations confirm that because of the extended conformation and the lack of hydrogen bonding of the peptide backbone, the peptides do not insert into the hydrophobic core of the water/cyclohexane or in the lipid bilayer systems, in agreement with calorimetric and NMR experimental data. The backbone of the peptide overlaps with the carbonyl distribution with the phospholipids. The peptides appear to perturb the atom distribution of the lipids, making the distribution of groups near the carbonyl area narrower.

The lysine peptides in the bilayer always form salt bridges between the Lys side chain and the C-terminus and starting from two different orientations end up in the same position and orientation in the bilayer. Arg in one case forms a long-lasting cation$-\pi$ interaction (15 out of 50 ns, as compared to 25 out of 50 ns salt bridge). Both lysine and arginine peptides are not as hydrophilic as expected because of stable electrostatic interactions in octanol and the bilayer. Although cation$-\pi$ interactions might not be the most favorable orientation in this particular peptide, their stability suggests that such interactions may play a role in other membrane binding peptides, most notably in short antimicrobial peptides with a high Arg and Trp content. The higher propensity of Arg−Trp cation$-\pi$ interactions as compared to Lys−Trp is consistent with statistical data on membrane proteins. We also found a significant fraction of Trp interactions with the positively charged lipid headgroup. Such interactions might play a role in the preference of Trp for the lipid/water interface region.

The simulations in this study have given an atomistic basis to the thermodynamics numbers for two of the 20 peptides, in different environments. Related simulations on the other peptides and free energy calculations of the 20 residues in water/octanol are now underway and will provide a thorough test for quantitative accuracy of the simulations and a means to improve the simulation methods. Clearly, many challenges for systematic studies of these peptides in the lipid−bilayer and water−octanol systems and the general understanding of the thermodynamic balance of membrane protein partitioning and folding still lie ahead.

REFERENCES

1. White, S. H., and Wimley, W. C. (1999) *Annu. Rev. Biophys. Biomol. Struct. 28*, 319−365.
2. Popot, J. L., and Engelman, D. M. (1990) *Biochemistry 29*, 4031−4037.
3. Popot, J. L., and Engelman, D. M. (2000) *Annu. Rev. Biochem. 69*, 881−922.
4. Wimley, W. C., Creamer, T. P., and White, S. H. (1996) *Biochemistry 35*, 5109−5124.
5. Wimley, W. C., Gawrisch, K., Creamer, T. P., and White, S. H. (1996) *Proc. Natl. Acad. Sci. U.S.A. 93*, 2985−2990.
6. Wimley, W. C., and White, S. H. (1996) *Nat. Struct. Biol. 3*, 842−848.
7. Kessel, A., and Ben-Tal, N. (2002) *Curr. Top. Membr. 52*, 205−253.
8. Hansson, T., Oostenbrink, C., and van Gunsteren, W. F. (2002) *Curr. Opin. Struct. Biol. 12*, 190−196.
9. Karplus, M. (2002) *Acc. Chem. Res. 35*, 321−323.
10. Tieleman, D. P., Marrink, S. J., and Berendsen, H. J. C. (1997) *Biochim. Biophys. Acta 1331*, 235−270.
11. Forrest, L. R., and Sansom, M. S. P. (2000) *Curr. Opin. Struct. Biol. 10*, 174−181.
12. Scott, H. L. (2002) *Curr. Opin. Struct. Biol. 12*, 495−502.
13. Chipot, C., and Pohorille, A. (1998) *J. Am. Chem. Soc. 120*, 11912−11924.
14. Chipot, C., Maigret, B., and Pohorille, A. (1999) *Proteins 36*, 383−399.
15. Wymore, T., and Wong, T. C. (1999) *Biophys. J. 76*, 1199−1212.
16. LaRocca, P., Biggin, P., Tieleman, D. P., and Sansom, M. S. P. (1999) *Biochim. Biophys. Acta 1462*, 185−200.
17. Shepherd, C. M., Vogel, H. J., and Tieleman, D. P. (2003) *Biochem. J. 370*, 233−243.
18. Yau, W. M., Wimley, W. C., Gawrisch, K., and White, S. H. (1998) *Biochemistry 37*, 14713−14718.
19. MacCallum, J. L., and Tieleman, D. P. (2002) *J. Am. Chem. Soc. 124*, 15085−15093.
20. Faraldo-Gomez, J. D., Smith, G. R., and Sansom, M. S. P. (2002) *Eur. Biophys. J. 31*, 217−227.
21. van Gunsteren, W. F., Kruger, P., Billeter, S. R., Mark, A. E., Eising, A. A., Scott, W. R. P., Huneberg, P. H., and Tironi, I. G. (1996) *Biomolecular simulation: the GROMOS96 manual and User Guide*, Biomos Hochschulverlag AG an der ETH Xurich, Groningen/Zurich.
22. Berendsen, H. J. C., van der Spoel, D., and van Drunen, R. (1995) *Comput. Phys. Commun. 91*, 43−56.
23. van der Spoel, D., van Buuren, A. R., Apol, E., Meulenhoff, P. J., Tieleman, D. P., Sijbers, A. L. T. M., Hess, B., Feenstra, K. A., Lindahl, E., van Drunen, R., and Berendsen, H. J. C. (2002) *Gromacs User manual υ 3.1*, Department of Biophysical Chemistry, University of Groningen, Groningen, The Netherlands.
24. Lindahl, E., Hess, B., and van der Spoel, D. (2001) *J. Mol. Model. 7*, 306−317.
25. Berger, O., Edholm, O., and Jahnig, F. (1997) *Biophys. J. 72*, 2002−2013.
26. Hermans, J., Berendsen, H. J. C., van Gunsteren, W. F., and Postma, J. P. M. (1984) *Biopolymers 23*, 1513−1518.
27. Hess, B., Bekker, H., Berendsen, H. J. C., and Fraaije, J. (1997) *J. Comput. Chem. 18*, 1463−1472.
28. Darden, T., York, D., and Pedersen, L. (1993) *J. Chem. Phys. 98*, 1463−1472.
29. Berendsen, H. J. C., Postma, J. P. M., van Gunsteren, W. F., DiNola, A., and Haak, J. R. (1984) *J. Chem. Phys. 81*, 3684−3690.
30. Feenstra, K. A., Hess, B., and Berendsen, H. J. C. (1999) *J. Comput. Chem. 20*, 786−798.
31. Humphrey, W., Dalke, A., and Schulten, K. (1996) *J. Mol. Graph. 14*, 33−38.
32. Chipot, C., Maigret, B., Pearlman, D. A., and Kollman, P. A. (1996) *J. Am. Chem. Soc. 118*, 2998−3005.
33. Daura, X., van Gunsteren, W. F., and Mark, A. E. (1999) *Proteins: Struct., Funct., Genet. 34*, 269−280.
34. Franks, N. P., Abraham, M. H., and Lieb, W. R. (1993) *J. Pharmacol. Sci. 82*, 466−470.
35. DeBolt, S. E., and Kollman, P. A. (1995) *J. Am. Chem. Soc. 117*, 5316−5340.
36. Tieleman, D. P., Forrest, L. R., Sansom, M. S. P., and Berendsen, H. J. C. (1998) *Biochemistry 37*, 17554−17561.
37. Hendsch, Z. S., and Tidor, B. (1994) *Protein Sci. 3*, 211−226.
38. Minoux, H., and Chipot, C. (1999) *J. Am. Chem. Soc. 121*, 10366−10372.
39. Mitchell, J. B. O., Nandi, C. L., McDonald, I. K., Thorton, J. M., and Price, S. L. (1994) *J. Mol. Biol. 239*, 315−331.
40. Gallivan, J. P., and Dougherty, D. A. (1999) *Proc. Natl. Acad. Sci. U.S.A. 96*, 9459−9464.
41. Glaser, F., Steinberg, D. M., Vakser, I. A., and Ben-Tal, N. (2001) *Proteins: Struct., Funct., Genet. 43*, 89−102.
42. Adamian, L., and Liang, J. (2001) *J. Mol. Biol. 311*, 891−907.
43. Schibli, D. J., Epand, R. F., Vogel, H. J., and Epand, R. M. (2002) *Biochem. Cell Biol. 80*, 667−677.
44. White, S. H. (2001) *Biophys. J. 80*, 20.
45. Grossfield, A., and Woolf, T. B. (2002) *Langmuir 18*, 198−210.
46. Woolf, T. B., Grossfield, A., and Pearson, J. G. (1999) *Int. J. Quantum Chem. 75*, 197−206.
47. Villa, A., and Mark, A. E. (2002) *J. Comput. Chem. 23*, 548−553.
48. Schuler, L. D., Daura, X., and van Gunsteren, W. F. (2001) *J. Comput. Chem. 22*, 1205−1218.
49. MacCallum, J. L., and Tieleman, D. P. (2003) *J. Comput. Chem.*, in press.
50. Tieleman, D. P., and Sansom, M. S. P. (2001) *Int. J. Quantum Chem. 83*, 166−179.

BI027001J